

## Mesogenic complementary absorbing dyads based on porphyrin and perylene units

Xiangfei Kong<sup>a</sup>, Hongkang Gong<sup>a</sup>, Shengping Dai<sup>a</sup>, Wei Yao<sup>a</sup>, Linping Mu<sup>\*b</sup>,  
Shufen Zhang<sup>a,c</sup> and Guixia Wang<sup>\*a</sup>

<sup>a</sup>College of Chemistry and Bioengineering, Guangxi Key Laboratory of Electrochemical and Magnetochemical Functional Materials, Guilin University of Technology, Jian'gan Road No. 12, Guilin 541006, China

<sup>b</sup>School of Physics and Information Engineering, Shanxi Normal University, Gongyuan Avenue No. 1, Linfen 041004, China.

<sup>c</sup>State Key Laboratory of Fine Chemicals, Dalian University of Technology, Linggong Road No. 2, Dalian 116024, China

*Dedicated to Professor Kazuchika Ohta on the occasion of his retirement*

Received 5 December 2017

Accepted 20 December 2017

**ABSTRACT:** Five novel dyads, consisting of a tetraphenylporphyrine unit connected to a perylene monoimide diester unit *via* a flexible bridge  $-\text{CONH}-(\text{CH}_2)_n-$  ( $n = 4, 6, 8, 10$  and  $12$ ), have been synthesized. Their structures were characterized by  $^{13}\text{C}$  and  $^1\text{H}$  nuclear magnetic resonance spectroscopy, infrared spectroscopy, mass spectrometry and elemental analysis. The UV-vis absorption spectra revealed these dyads have broad optical absorption in the ultraviolet and visible regions due to the complementary absorption of the two units. The differential scanning calorimetry traces and polarized optical microscopy textures showed all these dyads have columnar liquid crystal phases. Cyclic voltammetry revealed the highest occupied molecular orbitals of the dyads located on the porphyrin units, and the lowest unoccupied molecular orbitals located on the perylene units. In addition, these results were in agreement with that of the theoretical modeling. When excited at 423 or 473 nm, the photoluminescent emission spectra showed that the degree of fluorescence quenching of porphyrin units increased as the spacers became shorter. This quenching was ascribed to intramolecular photoinduced electron transfer, which also induced the dyad molecules to form the charge-separated states. The charge-separated molecules were further confirmed by the photocurrent response curves. These behaviors of broad absorption of the ultraviolet-visible light, yielding the charge-separated states of the molecules when excited and the formation of columnar liquid crystal phase made these dyads candidates for single-component photovoltaic active materials.

**KEYWORDS:** porphyrin, perylene, discotic liquid crystal, dyad, photoinduced electron transfer.

### INTRODUCTION

Organic solar cells (OSCs), featuring solution processing, light weight and mechanical flexibility, have attracted immense attention in the past decades [1–4]. At present, the state-of-the-art power conversion efficiency (PCE) for fullerene-based bulk heterojunction (BHJ) OSCs achieved 11–12% [5–7]. In recent years, non-fullerene acceptors have attracted much attention

because of their easily tunable molecular energy levels and excellent optical absorption properties [8, 9]. Recently [10], more than 13% PCE was obtained by blending a fluorinated  $\pi$ -conjugated polymer with a fluorinated fullerene-free small-molecule acceptor. In spite of these remarkable performances, the realization of solution-processed BHJ solar cells still poses a number of problems related to both the nature of the active materials and the fabrication process [11]. For example, the fine-control of phase separation and achieving high charge-carrier mobility in active layers are still very difficult with BHJ solar cells [2, 12, 13].

\*Correspondence to: Guixia Wang, email: 2010033@glut.edu.cn, tel.: +86 0773-8991-547, fax: +86 0773-8991-547; Linping Mu, email: mulinping6266@163.com.

As another interesting strategy, electron donor–acceptor dyad, triad, multiad and block copolymer molecules or all-in-one molecules where the electron donor (D) and acceptor (A) units are covalently linked in a single molecule have been reported for their potential as photovoltaic materials [12, 14–19]. These single-component photovoltaic materials possess multi-functions such as light harvesting, exciton dissociation and electron and hole transport. Moreover, several major advantages, such as a considerable simplification of device fabrication, stabilization of the morphology of the active material, and efficient (or fast) charge separation can be expected in the single-component OSCs [11]. At present, the PCE for single-component OSCs has surpassed 2% [12, 15, 17], which is lower than that of BHJ solar cells. This is because the design of electron donor–acceptor molecules for efficient single-component OSCs is in fact difficult. Some important prerequisites for solar cell applications, such as strong and broad optical absorption, the energy level matching of the donor and acceptor units, the prevention of charge recombination and the efficient transport of the separated charges to the electrodes, need to be considered and balanced [11].

Wasielewski proposed that the ideal functional organic materials used in solar cells should have electron donor and acceptor building blocks covalently attached in a single molecule, as well as the ordered arrangement of these building blocks in the solid state [13]. So far, the first aspect has been investigated as conventional single-component photovoltaic materials, while the second one is still a challenge and makes slow progress. However, the use of self-assembly strategy offers the opportunity to achieve the ordered structure and improved charge carrier mobility in the solid state [20, 21].

Calamitic and discotic liquid crystals (DLCs), featuring long exciton diffusion length and high charge-carrier mobility, have been considered as a new generation of organic photovoltaics [22]. The conventional DLC molecules comprise a planar rigid core and several

aliphatic chains, normally through ether, thioether, or ester bonds peripherally attached to the cores [23–25]. The majority of DLCs are thermotropic liquid crystals and have a strong tendency for columnar mesophase formation. Since there are strong  $\pi$ – $\pi$  interactions between adjacent cores within the same column, the carrier mobility is up to  $1 \text{ cm}^2 \cdot \text{V}^{-1} \cdot \text{s}^{-1}$  along the columnar axes [26, 27]. In addition, the peripheral side chains act as insulating layers, and the charge-carrier mobility is low in the direction perpendicular to the molecular column. Thus, the DLC materials exhibiting ordered columnar phases have application potential as one-dimensional charge carrier transport systems [28]. So far, the 4–8% PCE of bilayer solar cells and BHJ solar cells using DLC materials have been achieved [22].

The dyad, triad and multiad DLCs, containing D and A units and forming columnar phases, are an emerging single-component photovoltaic material. Since the so-called  $p$ – $n$  heterojunction exists at the molecular level, these D–A DLCs possess fast intramolecular photoinduced electron transfer and form charge separated states [29–33]. Some D–A DLCs yield dual pathways along molecular columns to transfer electrons and holes [34, 35]. At present, the discogens used in these D–A DLCs are limited in triphenylene, anthraquinone, perylene and BODIPY derivatives [36–42].

To use a wider range of the solar spectrum, dyads based on porphyrin and perylene units were designed in this work. Porphyrins have flat heterocyclic structure and a delocalized  $\pi$ -electron system, and are excellent light-harvesting compounds [43]. Porphyrin based compounds have attracted great interest in the fields of photodynamic therapy [44, 45], dye-sensitized [46, 47] and BHJ solar cells [48, 49]. While the perylene derivatives, possessing excellent photochemical and thermal stability, high fluorescence quantum yield, and multiple positions for chemical modification, were attractive candidate materials for OLEDs [50, 51] and OSCs [52–54], and several others. Herein,

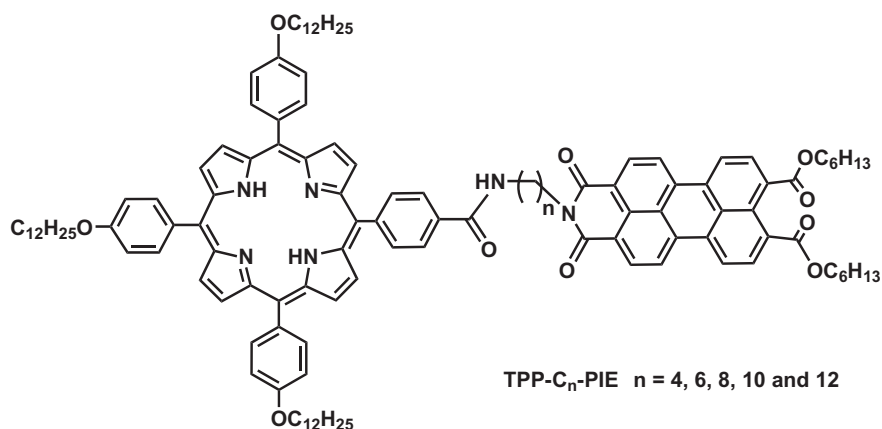


**Fig. 1.** Molecular structures of the dyads TPP-C<sub>n</sub>-PIE ( $n = 4, 6, 8, 10$  and  $12$ )

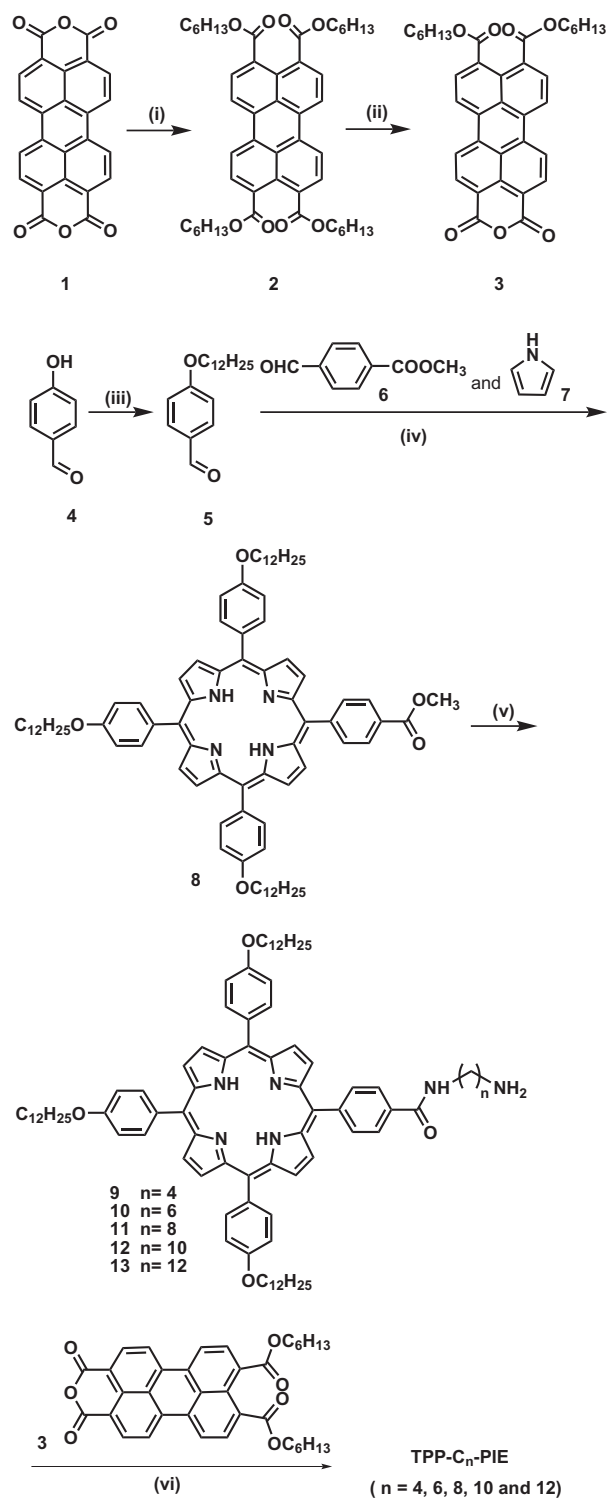
the dyads consisting of a tetraphenylporphyrin unit (absorption in the purple and yellow regimes) which was covalently linked to a perylene monoimide diester (PIE) unit (absorption in the green regime) were synthesized. The molecular structures of the dyads are shown in Fig. 1, denoted as **TPP-C<sub>n</sub>-PIE** ( $n = 4, 6, 8, 10$  and  $12$ ). The experimental results revealed that these dyads have broad optical absorption in the ultraviolet and visible region, and columnar liquid crystal phases as well.

## RESULTS AND DISCUSSION

### Synthesis

The synthetic routes are shown in Scheme 1. Tetrahexyl-perylene-tetracarboxylate (**2**) [55] and perylene-mono-anhydride-diester **3** [56] were synthesized in excellent yields according to the reports in the literature. Long chain aromatic aldehyde **5** [57] was prepared in quantitative yield, with no previous protection of the aldehyde moiety. The preparation of the porphyrin ester (**8**, **TPPE**) [58] was the key step towards asymmetric porphyrin derivative synthesis, which was obtained *via* the well-known Adler–Longo methodology [59]. The primary amine derivatives **9–13** were prepared by aminolysis reaction of **8** [60]. Since compounds **9–13** in solution were sensitive to air, they, without further purification, were condensed with **3** to give these dyads. In addition, the reference compound *N*-hexyl-perylene monoimide dihexyl esters (**PIE3**) was synthesized according to the previous report [33].

More specifically, the first step was the hydrolysis of perylene-3, 4, 9, 10-tetracarboxylic dianhydride (**1**) in basic aqueous solution to prepare the potassium perylene-3, 4, 9, 10-tetracarboxylate, then converted to **2** *via* an efficient phase-transfer catalysis method with methyl-trioctyl-ammonium chloride as a catalyst. Dihexyl-perylene-3, 4-anhydride-9, 10-dicarboxylate (**3**) was obtained as precipitate through acidic hydrolysis of **2** at one side in the mixed solvents of *n*-heptane and toluene. In the second step, **5** was prepared in quantitative yield *via* the alkylation of 4-hydroxybenzaldehyde (**4**) in the presence of anhydrous potassium carbonate, in DMF at 80 °C. **8** was prepared through the condensation reaction between **5**, methyl 4-formylbenzoate (**6**) and pyrrole (**7**) in the mixed solvent of xylol and 3-nitrobenzoic acid at 140 °C. Then **8** underwent an aminolysis reaction with excess alkane- $\alpha$ ,  $\omega$ -diamines, which also acted as solvents, to give **9–13**. The dyads were synthesized by the imidization reaction between **3** and the primary amine derivatives in imidazole at 130 °C, as dark red solids. The yields of the imidization reaction were 33–40%, which were attributed to the instability of the compounds **9–13**.



**Scheme 1.** Synthesis of dyads **TPP-C<sub>n</sub>-PIE** ( $n = 4, 6, 8, 10$  and  $12$ ). Reagents and conditions: (i) a. KOH, H<sub>2</sub>O, 75 °C, 1.5 h, b. HCl, pH = 8–9, C<sub>6</sub>H<sub>13</sub>Br, methyl trioctyl ammonium chloride, reflux, 6 h, 57%; (ii) toluene/heptane = 1/5, *p*-toluenesulfonic acid, 95 °C, 5 h, 79%; (iii) C<sub>12</sub>H<sub>25</sub>Br, K<sub>2</sub>CO<sub>3</sub>, DMF, 80 °C, 12 h, 98%; (iv) xylol, 3-nitrobenzoic acid, 140 °C, 3.5 h, 28%; (v) NH<sub>2</sub>(CH<sub>2</sub>)<sub>n</sub>NH<sub>2</sub>, ( $n = 2, 4, 6, 8, 10$  and  $12$ ), 100 °C, 22–48 h, 82–88%; (vi) imidazole, 130 °C, 5 h, 33–40%

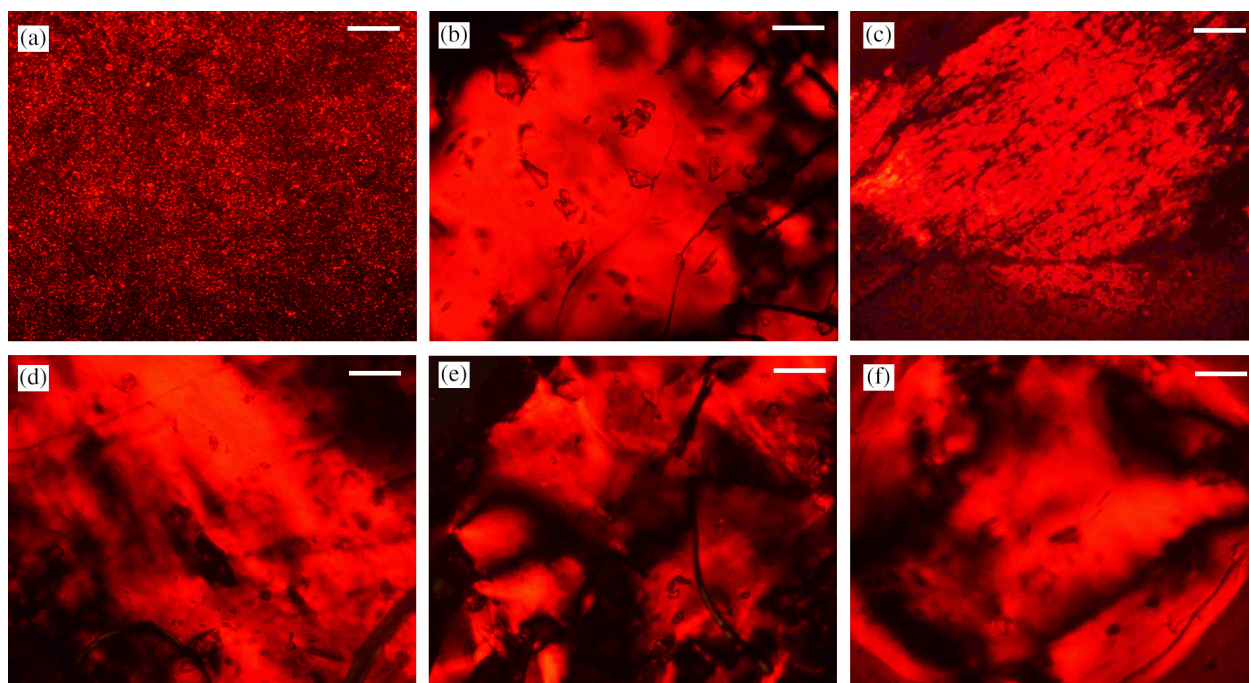


**Fig. 2.** Optical texture of **TPP-C<sub>12</sub>-PIE** (a, on heating at 117 °C) and POM microphotographs of **TPP-C<sub>12</sub>-PIE** (b), **TPP-C<sub>10</sub>-PIE** (c), **TPP-C<sub>8</sub>-PIE** (d), **TPP-C<sub>6</sub>-PIE** (e), **TPP-C<sub>4</sub>-PIE** (f) (observed in the cooling processes from the isotropic liquid at room temperature after applying mechanical stress, the scale bars are 50  $\mu\text{m}$ , crossed polarizers)

### Phase behaviors and potential in self-organization

Phase behaviors of the dyads were investigated by polarized optical microscopy (POM, see Fig. 2) and the differential scanning calorimetry (DSC, see Fig. 3 and Figs S1–S5 in the supplementary information). Peak transition temperatures along with the associated enthalpy changes ( $\Delta H$ ) are listed in Table 1. As shown in Fig. 3 and Fig. S1, **TPP-C<sub>12</sub>-PIE** showed two endothermic transitions and peaked at 68 and 114 °C in the first heating cycle, and one exothermic peak at 68 °C during the first cooling cycle. Under microscopic observation, the birefringent waxy solid was deformed when squeezed at room temperature. When heated, the birefringent fluid started to flow at 100 °C, and the birefringent phenomenon disappeared at 128 °C. The optical texture observed at 117 °C showed it had a columnar liquid crystal phase (see Fig. 2a). When cooled, the isotropic liquid cannot flow at 60 °C. In addition, the weak birefringent phenomenon resorted at room temperature. After applying mechanical stress, the birefringent phenomenon can be seen clearly (see Fig. 2b). It is believed that when cooled from the isotropic liquid, the molecules of the dyad self-assemble and arrange in face-on alignment on the slides (in which the molecular columns are perpendicular to the surface of the slide).

During the first heating run, **TPP-C<sub>10</sub>-PIE** showed one endothermic transition which peaked at 93 °C. During the first cooling cycle, one broad exothermic peak occurred at 74 °C (see Table 1 and Fig. S2). Under microscopic observation, the birefringent waxy solid was deformed

when squeezed at room temperature. When heated, the red fluid started to flow at 90 °C with birefringence, which was maintained until 105 °C. Upon cooling, the isotropic liquid cannot flow at 70 °C, the birefringence did not restore until room temperature. After applying mechanical stress, the birefringent phenomenon can be visualized expressly (see Fig. 2c).

In the first heating circle, **TPP-C<sub>8</sub>-PIE** showed three endothermic transitions which peaked at 78, 105 and 119 °C. During the first cooling cycle, one broad exothermic transition peaked at 87 °C (see Table 1 and Fig. S3). Under microscopic observation, the birefringent waxy solid was deformed when pressed at room temperature. When heated the red fluid started to flow at 105 °C with birefringence, which disappeared at 123 °C with continued heating. Upon cooling, the isotropic liquid cannot run at 80 °C, and the birefringence did not appear until room temperature. When squeezed, the birefringent phenomenon can be seen clearly (see Fig. 2d).

DSC curves showed two endothermic peaks at 78 and 111 °C in the heating cycle for **TPP-C<sub>6</sub>-PIE**, and one exothermic peak at 99 °C during the first cooling (see Table 1 and Fig. S4). Under microscopic observation, the birefringent waxy solid was deformed when squeezed at room temperature. When heated, the red fluid started to flow at 110 °C with birefringence, and it disappeared at 125 °C. When cooled, the isotropic liquid cannot run at 92 °C and the birefringence was not present until room temperature. When pressed, the birefringent phenomenon could be readily observed (see Fig. 2e).

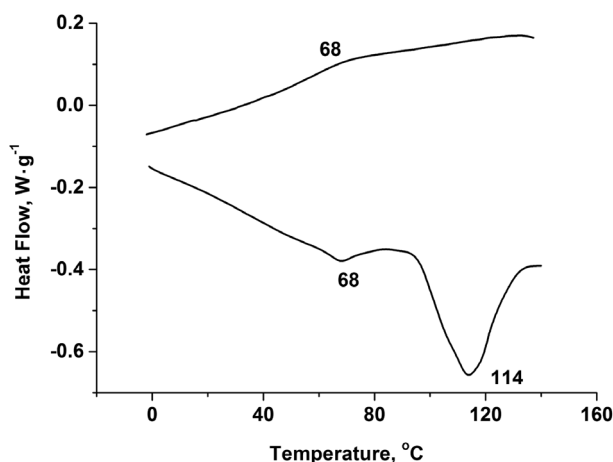


**Fig. 3.** DSC traces of **TPP-C<sub>12</sub>-PIE** (The downward peaks are characteristic of endothermic events; first heating and cooling cycle, peak temperatures labeled, at the scan rate of  $10^{\circ}\text{C}\cdot\text{min}^{-1}$ )

**TPP-C<sub>4</sub>-PIE** showed two endothermic transitions and peaked at 78 and 114 °C in the first heating cycle, and one exothermic peak at 104 °C during the first cooling cycle (see Table 1 and Fig. S5). Under microscopic observation, the birefringent waxy solid was deformed when pressed at room temperature. When heated, the birefringent fluid cannot run until 115 °C, and the birefringent phenomenon disappeared at 130 °C. When cooled, the isotropic liquid cannot flow at 99 °C and the birefringence did not resort until room temperature. When pushed, the birefringent phenomenon can be seen clearly (see Fig. 2f).

### Electrochemical behaviors and HOMO/LUMO energy levels

The electrochemical behaviors of the reference compounds **TPPE** and **PIE3**, and the dyads **TPP-C<sub>10</sub>-PIE** were studied by cyclic voltammetry (CV) in dry acetonitrile with  $0.1\text{ mol}\cdot\text{L}^{-1}$  tetrabutylammonium hexafluorophosphate (TBAPF6) as the supporting electrolyte. The experiments were performed at room temperature, using a standard three-electrode cell with a glass carbon electrode as the working electrode, a platinum wire as the counter electrode and an Ag/AgCl electrode as the

reference electrode. The scan rate was  $50\text{ mV}\cdot\text{s}^{-1}$ . For all CV measurements, the ferrocene/ferrocenium (Fc/Fc<sup>+</sup>) redox couples were used for calibration [61].

The cyclic voltammograms of **TPPE**, **PIE3** and **TPP-C<sub>10</sub>-PIE** are shown in Fig. 4. The HOMO energy values of these compounds were obtained from the potential values corresponding to the onsets of the first oxidation waves (denoted as  $E_{\text{ox}}(1)$ ). The  $E_{\text{ox}}(1)$  of **TPPE**, **PIE3** and **TPP-C<sub>10</sub>-PIE** were 1.24, 1.75 and 1.15 V, respectively. In addition, the potential value of the dyad corresponding to the onset of the second oxidation wave (denoted by  $E_{\text{ox}}(2)$ ) was 1.59 V. Analysis of these data showed that the first and second oxidation waves of the dyads can be assigned to the oxidation reactions of the porphyrin unit and the perylene unit, respectively.

Calibrated with the Fc/Fc<sup>+</sup> redox system, the HOMO energy value of each compound was estimated by the equation  $\text{HOMO (eV)} = -[e(E_{\text{ox}}(1) - E(\text{Fc/Fc}^+)) + 4.8]$  [30]. Thus, the HOMO values of **TPPE**, **PIE3** and **TPP-C<sub>10</sub>-PIE** were -5.50, -5.95 and -5.51 eV, respectively. The LUMO value of a compound can be estimated from the optical band gap (denoted as  $E_{\text{g}}$ ) and the HOMO value by the equation  $\text{LUMO} = \text{HOMO} + E_{\text{g}}$  [30]. The  $E_{\text{g}}$  was inferred from the onset of the longest wavelength absorption band. The  $E_{\text{g}}$  values of **TPPE** and **PIE3**, inferred from the onsets of the absorption spectra (Fig. 6), were 1.86 and 2.30 eV, respectively. Thus, the LUMO values of **TPPE** and **PIE3** were -3.64 and -3.65 eV, respectively. As we know, the LUMO of a dyad linked by a flexible spacer is coincident with the lower one of the two units [30]. Thus, the HOMO value (-5.95 eV), corresponding to  $E_{\text{ox}}(2)$ , and  $E_{\text{g}}$  (2.30 eV) of perylene unit should be used in the equation  $\text{LUMO} = \text{HOMO} + E_{\text{g}}$ , and the LUMO value of **TPP-C<sub>10</sub>-PIE** is -3.65 eV. In this way, the  $E_{\text{g}}$  of **TPP-C<sub>10</sub>-PIE** equals 1.86 eV.

The electronic structures of the cores of **TPP-C<sub>10</sub>-PIE** were modeled using the Gaussian 16 suite of programs. Since the side chains have little effect on the HOMO and LUMO values of DLCs [62], the alkyl chains were all replaced by methyl groups in the computer simulations to reduce the computational load. Full geometry optimization of the dyad were performed at the density

**Table 1.** Phase behaviors of **TPP-C<sub>n</sub>-PIE** ( $n = 4, 6, 8, 10$  and  $12$ ). Phase transition temperatures (peak, °C) and associated enthalpy changes ( $\text{J}\cdot\text{g}^{-1}$ , in parentheses) determined by DSC at the scan rate  $10^{\circ}\text{C}\cdot\text{min}^{-1}$ , under  $N_2$

Compounds	First heating scan, temperatures (°C) ( $\Delta H$ ( $\text{J}\cdot\text{g}^{-1}$ ))	First cooling scan, temperatures (°C) ( $\Delta H$ ( $\text{J}\cdot\text{g}^{-1}$ ))
<b>TPP-C<sub>12</sub>-PIE</b>	Col1 <sup>a</sup> 68 (0.70) Col2 <sup>a</sup> 114 (15.76) I <sup>a</sup>	I <sup>a</sup> 68 (0.67) Col <sup>a</sup>
<b>TPP-C<sub>10</sub>-PIE</b>	Col1 93 (6.71) I	I 74 (0.52) Col
<b>TPP-C<sub>8</sub>-PIE</b>	Col1 78 (0.16) Col2 105 (0.35) Col3 <sup>a</sup> 119 (1.08) I	I 87 (0.38) Col
<b>TPP-C<sub>6</sub>-PIE</b>	Col1 78 (1.84) Col2 111 (0.38) I	I 99 (0.32) Col
<b>TPP-C<sub>4</sub>-PIE</b>	Col1 78 (0.52) Col2 114 (0.12) I	I 104 (0.32) Col

<sup>a</sup> Col1, Col2, Col3 and Col: columnar liquid crystal phase; I: isotropic liquid.

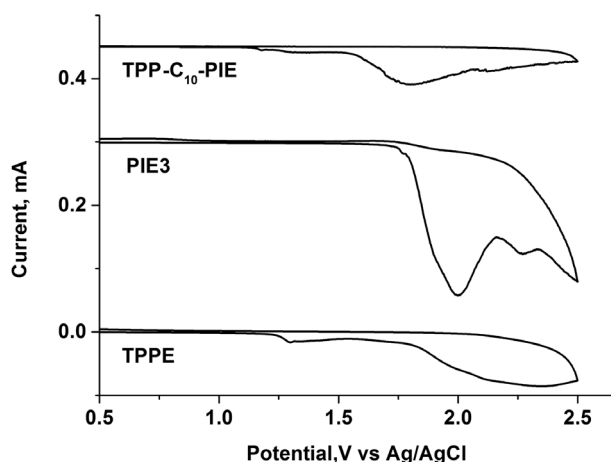


**Fig. 4.** Cyclic voltammograms of compounds **TPPE**, **PIE3** and **TPP-C<sub>10</sub>-PIE** at room temperature (drop casted films,  $0.1 \text{ mol} \cdot \text{L}^{-1}$  in acetonitrile solution of TBAPF<sub>6</sub>, at the scan rate of  $50 \text{ mV} \cdot \text{s}^{-1}$ ). In order to facilitate the observation, the curves of **PIE3** and **TPP-C<sub>10</sub>-PIE** moved up 0.3 and 0.45 mA, respectively

functional theory (DFT) level using Becke's three-parameter B3LYP exchange functional and the 6-31G basis set. The geometry of the dyad was optimized in dichloromethane (DCM), and its isosurfaces of the frontier molecular orbital are illustrated in Fig. 5. It can be seen that the dyad molecule tends to exist in extended conformations in dilute DCM solution, and the HOMO and LUMO orbitals of the dyad are located on the porphyrin and perylene units, respectively. The HOMO, LUMO and  $E_g$  values were predicted to be -5.12, -3.35 and 1.77 eV, respectively, which matched the measured values.

### Steady-state spectroscopy

**UV-vis absorption spectra.** UV-vis absorption spectra of the **TPPE**, **PIE3**, the mixture of **TPPE** and **PIE3** (in the molar ratio of 1:1), and the dyads **TPP-C<sub>n</sub>-PIE** ( $n = 4, 6, 8, 10$  and  $12$ ) were studied in DCM solutions ( $5 \times 10^{-6} \text{ mol} \cdot \text{dm}^{-3}$ ) (Fig. 6). **PIE3** has optical absorption from 250 to 540 nm. In the ultraviolet region, its absorption maximum is at 263 nm, and the peak optical density corresponds to an extinction coefficient ( $\epsilon$ ) of  $4.56 \times 10^4 \text{ L} \cdot \text{mol}^{-1} \cdot \text{cm}^{-1}$ , belonging to the transition of  $n-\pi^*$  of C=O groups [33]. In the visible region, it has a maximum absorption at 507 nm ( $\epsilon = 5.48 \times 10^4 \text{ L} \cdot \text{mol}^{-1} \cdot \text{cm}^{-1}$ ) with two vibronic bands at 475 and 450 nm, correlated to the  $\pi-\pi^*$  electron transitions. **TPPE** shows characteristic I-IV Q bands (652, 596, 557 and 517 nm) and one strong Soret band (422 nm,  $\epsilon = 4.88 \times 10^5 \text{ L} \cdot \text{mol}^{-1} \cdot \text{cm}^{-1}$ ), belonging to the  $\pi-\pi^*$  electron transitions of the porphyrin ring [63].

The absorption spectrum of the mixture of **TPPE** and **PIE3** (in the molar ratio of 1:1), retained the Soret and I-IV Q bands of **TPPE** and the vibronic bands of **PIE3**,

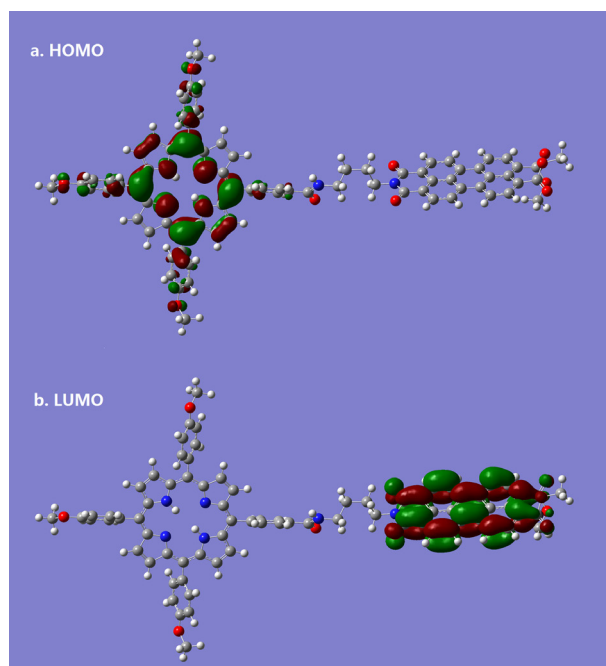


**Fig. 5.** Optimized geometric structure of **TPP-C<sub>10</sub>-PIE** in DCM and its frontier orbitals calculated by density functional theory (DFT) at the B3LYP/6-31G level

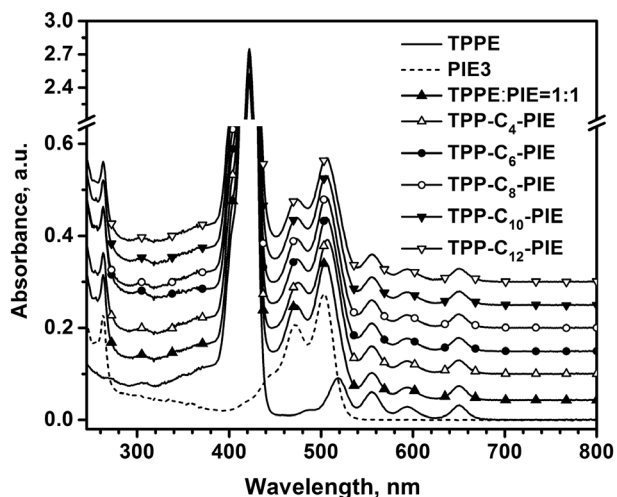


**Fig. 6.** UV-vis absorption spectra of **TPPE**, **PIE3**, the mixture of **TPPE** and **PIE3** (in the molar ratio of 1:1), and **TPP-C<sub>n</sub>-PIE** ( $n = 4, 6, 8, 10$  and  $12$ ) in DCM,  $c = 5 \times 10^{-6} \text{ mol} \cdot \text{dm}^{-3}$ . In order to facilitate the observation, the curves of the mixture, **TPP-C<sub>4</sub>-PIE**, **TPP-C<sub>6</sub>-PIE**, **TPP-C<sub>8</sub>-PIE**, **TPP-C<sub>10</sub>-PIE** and **TPP-C<sub>12</sub>-PIE** were successively moved up 0.05 unit

is a superimposition of the two monomeric spectra. This shows that there is no charge transfer between the **TPPE** and **PIE3** molecules in the ground states in dilute DCM solution. The absorption spectra of the dyads are almost identical to that of the mixture of **TPPE** and **PIE3** (in the molar ratio of 1:1), showing that in the ground states the electronic coupling between the two units of a dyad is

weak. In summary, the absorption spectra of the dyads cover the ultraviolet and visible regions of the solar spectrum due to the complementary absorption of the porphyrin and perylene units.

**Photoluminescent emission spectra.** Photoluminescent emission spectra of the dyads were measured in DCM solutions ( $c = 5 \times 10^{-6} \text{ mol} \cdot \text{dm}^{-3}$ ) at 423 and 473 nm, which correspond to the optical absorptions of the Soret band of the porphyrin unit and the perylene unit, respectively. As a comparison, the emission of the reference compounds **TPPE** and **PIE3** were also measured.

Excited at 423 nm, **PIE3** has characteristic fluorescence emissions between 490 and 700 nm, with one peak at 528 nm and two shoulders at 559 and 622 nm (see Fig. 7). The fluorescence emissions of **TPPE** is between 630 and 780 nm, with the peak at 662 nm and one shoulder at 728 nm. The peak intensity of **TPPE** is about one fifth of that of **PIE3**. Compared with **TPPE**, the spectra profiles of **TPP-C<sub>n</sub>-PIE** ( $n = 4, 6, 8, 10$  and  $12$ ) are very similar. The fluorescence emission of the perylene units of the dyads is completely quenched. This is attributed to the Förster and Dexter type energy transfer from the perylene units to the porphyrin units, since the fluorescence emission region of the perylene unit (490–700 nm) is overlapped with the Q-bands of porphyrin (480–680 nm), and the lengths of the bridges of the dyads are less than 10 angstroms. Thus, the porphyrin units acquiring energy from the perylene units should have a stronger fluorescence emission than that of **TPPE**. However, the emission intensity of the highest peaks of the dyads decrease as compared with that of **TPPE**, and a further decrease is found as the flexible spacers get shorter. This implies there are additional electron transfer processes between the porphyrin and perylene units,

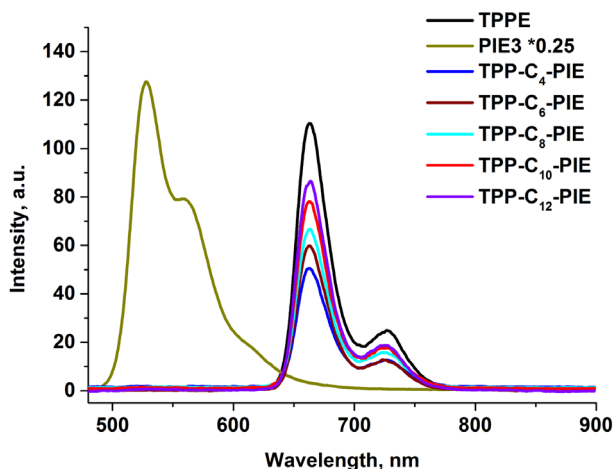


**Fig. 7.** Fluorescence emission spectra of **TPPE**, **PIE3** and **TPP-C<sub>n</sub>-PIE** ( $n = 4, 6, 8, 10$  and  $12$ ) in DCM ( $c = 5 \times 10^{-6} \text{ mol} \cdot \text{dm}^{-3}$ ,  $\lambda_{\text{ex}} = 423 \text{ nm}$ , the intensity of **PIE3** plotted here was a quarter of its original value)

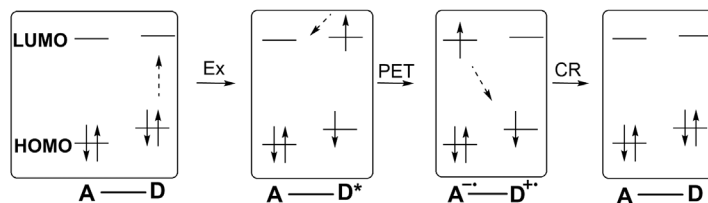


**Fig. 8.** Schematic representation of the photoinduced electron transfer of **TPP-C<sub>10</sub>-PIE** ( $\lambda_{\text{ex}} = 423 \text{ nm}$ , a dashed arrow indicates the two energy levels involving one transition or transfer of an electron)

which are responsible for the fluorescence quenching of the porphyrin units.

The fluorescence quenching of the porphyrin units can be explained by the photoinduced electron transfer theory [64]. The electron-rich porphyrin units and the electron-deficient perylene units act as the electron D and A, and were looked at as entities that could be studied separately. To simplify these processes, the HOMO and LUMO values of the D and A units are assumed to be fixed. In the case of **TPP-C<sub>10</sub>-PIE**, the energetic positions of the HOMO and LUMO energy levels are shown schematically in Fig. 8.

When the D unit was excited, the electron transfer processes of the dyad were depicted in Fig. 8. Before excitation, the dyad molecule was in the ground state (indicated by A–D). When the D unit was excited (represented by Ex), an electron transitioned from the HOMO to the LUMO to give a molecule with the D unit in the excited state (denoted by A–D\*). Since the LUMO level of the D unit was higher than that of the A unit, and the core of the A unit was deficient in electrons, the electron in the LUMO of the D transferred to A, yielding a molecule in charge transfer state (denoted by A\*–D\*). This was a photoinduced electron transfer process (represented by PET). In the end, the electron on the LUMO level of the A unit transferred to the HOMO level of the D unit, and then two units returned to the original ground state. This process was a charge recombination process (expressed by CR). In the above processes, the PET was a key step leading to fluorescence quenching. According to the theory of photoinduced electron transfer, the electron transfer rate constant decays exponentially with the distance between the D and A units [64]. Thus, the shorter the bridges are, the stronger the fluorescence quenching degrees of the D units are.

Excited at 473 nm, the profiles of fluorescence emission spectra of **PIE3** and **TPPE** were similar to that when they were excited at 423 nm, respectively (Fig. 9), while the fluorescence emission of the featured dyads has the characteristics of both **PIE3** and **TPPE**. Since there were the Förster and Dexter type energy transfer from the perylene units to the porphyrin units, the fluorescence emission of the perylene units of the dyads was quenched, and the emission of the porphyrin units was enhanced. It also can be seen that the peak intensities of the porphyrin

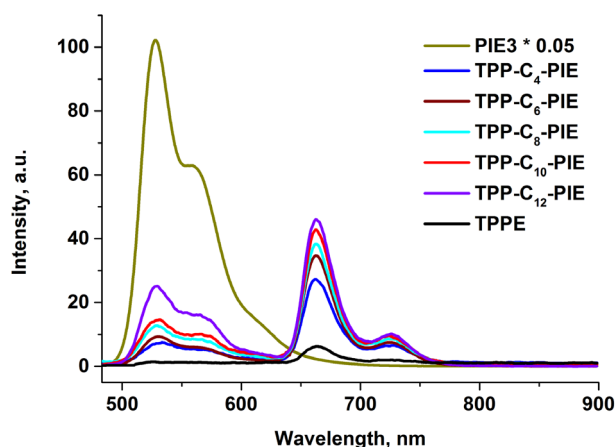


**Fig. 9.** Fluorescence emission spectra of TPPE, PIE3 and TPP-C<sub>n</sub>-PIE ( $n = 4, 6, 8, 10$  and  $12$ ) in DCM ( $c = 5 \times 10^{-6}$  mol · dm<sup>-3</sup>,  $\lambda_{\text{ex}} = 473$  nm. The intensity of PIE3 plotted here was five percent of its original value)

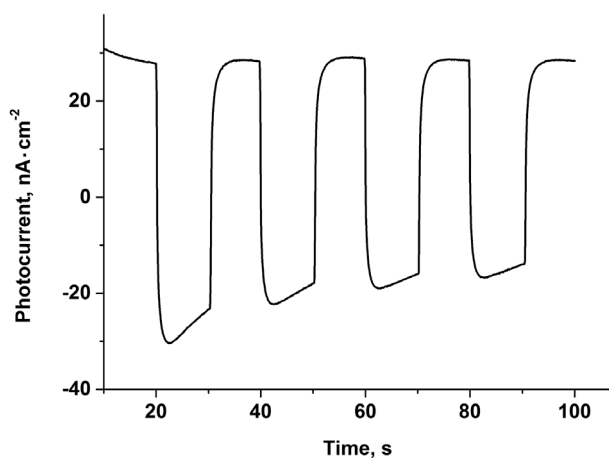


**Fig. 10.** Photocurrent curve of TPP-C<sub>10</sub>-PIE film polarized at +0.10 V and irradiated with intermittent white light (counter electrode: platinum wire; reference electrode: Ag/AgCl electrode; working electrode: ITO glass coated with TPP-C<sub>10</sub>-PIE; supporting electrolyte: KCl aqueous solution,  $c = 0.1$  mol · dm<sup>-3</sup>)

units decreased as the flexible linkers got shorter. The fluorescence quenching of the porphyrin units is also attributed to the photoinduced electron transfer, just as that they were quenched at 423 nm.

### Photocurrent phenomena

The photocurrent generation of TPP-C<sub>10</sub>-PIE film, deposited on an indium tin oxide (ITO) glass electrode, was tested using a standard three-electrode cell. The film on the working electrode was fabricated by the drop-casting method. Using 63.2 mW · cm<sup>-2</sup> intermittent white light irradiation and applying a voltage of +0.1 V to the working electrode, a rapid anodic photocurrent response was observed (Fig. 10).

When the TPP-C<sub>10</sub>-PIE film was irradiated with white light, the molecules in charge-separated state, TPP<sup>•+</sup>-C<sub>10</sub>-PIE<sup>•-</sup>, were yielded due to the intramolecular photoinduced electron transfer (see Fig. 8). The negatively charged perylene unit gave electrons to the conduction band of ITO, which resulted in the anodic photocurrent.

## EXPERIMENTAL

### Materials

All reagents and solvents were from Aladdin Industrial Corporation, Macklin Inc., XiLong Chemical and FuYu Chemical. All were analytically pure and used without further purification if not specified.

### Characterization and instrumentation

IR was performed on a VECTOR 22 FT-IR spectrometer (KBr tablet). <sup>1</sup>H NMR spectra were recorded on a Bruker spectrometer (500 MHz). Mass spectra were obtained on an Agilent ESI 6400 mass spectrometer. EA was recorded on a Thermo Flash EA-1112 instrument. DSC experiments were carried out on a Thermal Analysis DSC-Q100 instrument. The mesomorphic properties were evaluated by a polarized optical microscopy instrument (Olympus THMS600) provided with a heating stage (Linkam THMSE 600). CV and photocurrent curves were performed on a Shanghai Chen Hua CHI760E electrochemical workstation. Geometry optimization of the dyad was performed by Gaussian 16 program package. UV-vis absorption spectra were recorded on a Shimadzu UV-2450 spectrometer. Fluorescence emissions were performed on a HITACHI F-4600 instrument.

### Synthesis

**Synthesis of tetrahexyl perylene-3,4,9,10-tetracarboxylate (2).** The solution of **1** (0.95 g, 2.42 mmol) and potassium hydroxide (2.63 g, 46.9 mmol) in water (300 mL) was filtered after stirring at 70 °C for 1.5 h. The filtrate was acidified with HCl (*ca.* 1 mol · L<sup>-1</sup>) until the pH was 8–9. Then 1-bromohexane (4.2 g, 25.2 mmol) and methyl-trioctyl-ammonium chloride (1 g, 0.2 mmol) were added to the solution. The reaction mixture was then refluxed for 6 h under vigorous stirring, then cooled to room temperature, and filtered. The filter cake was washed with ethanol (35 mL) three times to give **2** as a yellow solid. Yield 1.05 g (57%). <sup>1</sup>H NMR (500 MHz; CDCl<sub>3</sub>; Me<sub>4</sub>Si):  $\delta_{\text{H}}$ , ppm 0.91 (12H, t, -CH<sub>3</sub>), 1.37–1.35 (16H, m, -CH<sub>2</sub>-), 1.48–1.42 (8H, m, -CH<sub>2</sub>-), 1.83–1.78 (8H, m, -O-CH<sub>2</sub>-CH<sub>2</sub>-), 4.33 (8H, t, -O-CH<sub>2</sub>-), 7.96–7.91 (4H, m, Ar-H), 8.13–8.06 (4H, m, Ar-H).

**Synthesis of dihexyl-perylene-3,4-anhydride-9,10-dicarboxylate (3).** **2** (4 g, 5.23 mmol) was added to the mixed solvent of toluene (3.0 mL) and heptane (15 mL). When heated to 80 °C the mixture became clear.

A red slurry was obtained after the reaction mixture reacted with *p*-toluene sulfonic acid (1.04 g, 5.47 mmol) at 95 °C for 5 h. After cooling to room temperature, the red solid was collected by filtration. The wet filter cake was recrystallized twice from DCM (24 mL) and methanol (40 mL), to give **3** as a red solid. Yield 2.39 g (79%). <sup>1</sup>H NMR (500 MHz; CDCl<sub>3</sub>; Me<sub>4</sub>Si): δ<sub>H</sub>, ppm 0.91 (6H, t, -CH<sub>3</sub>), 1.38–1.34 (8H, m, -CH<sub>2</sub>-), 1.49–1.44 (4H, m, -CH<sub>2</sub>-), 1.84–1.78 (4H, m, -O-CH<sub>2</sub>-CH<sub>2</sub>-), 4.35 (4H, t, -O-CH<sub>2</sub>-), 8.12 (2H, d, Ar-H), 8.48 (4H, t, Ar-H), 8.62 (2H, d, Ar-H).

**Synthesis of 4-(dodecyloxy)benzaldehyde (5).** **4** (2.44 g, 20 mmol), 1-bromododecane (6.72 g, 26.9 mmol) and anhydrous potassium carbonate (5.52 g, 40 mmol) were added to dried DMF (20 mL). Under nitrogen, the mixture was stirred at 80 °C for 12 h, then cooled to room temperature and diluted with water (100 mL). After extraction with DCM (4 × 30 mL), the combined organic layer was washed with brine (20 mL) and then dried (Na<sub>2</sub>SO<sub>4</sub>). After the solvent was removed at reduced pressure, the oily product obtained was purified by column chromatography (silica gel, DCM/petroleum ether, 1/2 v/v) to give **5** as a yellow oil. Yield 5.75 g (98%). <sup>1</sup>H NMR (500 MHz; CDCl<sub>3</sub>; Me<sub>4</sub>Si): δ<sub>H</sub>, ppm 0.88 (3H, t, -CH<sub>3</sub>), 1.37–1.23 (16H, m, -CH<sub>2</sub>-), 1.49–1.43 (2H, m, -CH<sub>2</sub>-), 1.83–1.77 (2H, m, -O-CH<sub>2</sub>-CH<sub>2</sub>-), 4.04 (2H, t, -O-CH<sub>2</sub>-), 6.99 (2H, d, Ar-H), 7.83 (2H, d, Ar-H), 9.88 (1H, s, -CHO).

**Synthesis of methyl 4-(10,15,20-tris(4-(dodecyloxy)phenyl)porphyrin-5-yl)benzoate (8, TPPE).** One solution of **5** (5.88 g, 21 mmol) and **6** (1.19 g, 6.7 mmol) in the mixture of 3-nitrobenzoic acid (1.85 g, 13.5 mmol) and xylol (32 mL) was heated to 140 °C. The other solution of pyrrole (1.805 g, 26.9 mmol) in xylol (32 mL) was slowly added to the first in 0.5 h. The mixture was then stirred at 140 °C for another 3.5 h. After evaporation of the xylol *in vacuo*, the crude product was purified by column chromatography (silica gel, DCM/petroleum ether, 1/2–1/1 v/v), then recrystallized from dichloromethane (10 mL) and methanol (10 mL) to give **8** as a purple solid. Yield 2.28 g (28%). <sup>1</sup>H NMR (500 MHz; CDCl<sub>3</sub>; Me<sub>4</sub>Si): δ<sub>H</sub>, ppm -2.75 (2H, s, pyrrole-NH), 0.90 (9H, t, -CH<sub>3</sub>), 1.49–1.31 (48H, m, -CH<sub>2</sub>-), 1.65–1.58 (6H, m, -CH<sub>2</sub>-), 2.01–1.94 (6H, m, -CH<sub>2</sub>-), 4.10 (3H, s, -COOCH<sub>3</sub>), 4.23 (6H, t, -O-CH<sub>2</sub>-), 7.26 (6H, d, Ar-H), 8.10 (6H, d, Ar-H), 8.30 (2H, d, Ar-H), 8.43 (2H, d, Ar-H), 8.76 (2H, d, Ar-H), 8.88 (6H, d, Ar-H).

**Synthesis of N-(4-aminobutyl)-4-(10,15,20-tris(4-(dodecyloxy)phenyl)porphyrin-5-yl)benzamide (9).** Under nitrogen, the solution of **8** (0.7 g, 0.57 mmol) in butane-1,4-diamine (3 g) was stirred at 100 °C for 22 h, allowed to cool to room temperature and then diluted with H<sub>2</sub>O (30 mL). After extraction with DCM (4 × 15 mL), the combined organic layers were washed with brine (15 mL) and then dried (Na<sub>2</sub>SO<sub>4</sub>). The solvent was removed *in vacuo*. The crude product was purified by column chromatography (silica gel, DCM/methanol,

10/1–5/1 v/v), to give **9** as a purple solid. However, the TLC showed that part of **9** had decomposed in this process. Thus, it was condensed with **3** as soon as possible to give **TPP-C<sub>4</sub>-PIE**.

**Synthesis of N-(6-aminohexyl)-4-(10,15,20-tris(4-(dodecyloxy)phenyl)porphyrin-5-yl)benzamide (10).** The same procedure as for **9** with hexane-1,6-diamine (3 g). The crude product as a purple solid without further purification was condensed with **3** to yield **TPP-C<sub>6</sub>-PIE**.

**Synthesis of N-(8-amino-octyl)-4-(10,15,20-tris(4-(dodecyloxy)phenyl)porphyrin-5-yl)benzamide (11).** The same procedure as for **9** with octane-1,8-diamine (3 g). The crude product as a purple solid without further purification was condensed with **3** to yield **TPP-C<sub>8</sub>-PIE**.

**Synthesis of N-(10-aminodecyl)-4-(10,15,20-tris(4-(dodecyloxy)phenyl)porphyrin-5-yl)benzamide (12).** The same procedure as for **9** with decane-1,10-diamine (3 g). The crude product as a purple solid without further purification was condensed with **3** to yield **TPP-C<sub>10</sub>-PIE**.

**Synthesis of N-(12-aminododecyl)-4-(10,15,20-tris(4-(dodecyloxy)phenyl)porphyrin-5-yl)benzamide (13).** The same procedure as for **9** with dodecane-1,12-diamine (3 g). The crude product as a purple solid without further purification was condensed with **3** to yield **TPP-C<sub>12</sub>-PIE**.

**Synthesis of TPP-C<sub>4</sub>-PIE.** Under nitrogen, the mixture of **9** (0.63 g, 0.53 mmol) and **3** (0.37 g, 0.63 mmol) in imidazole (10 g) was stirred at 130 °C for 5 h, allowed to cool to room temperature and then diluted with hot H<sub>2</sub>O (20 mL). The red solid was collected by filtration, and purified by column chromatography (silica gel, DCM/ethyl acetate, 15/1–5/1 v/v), to give the title compound as a red solid. Yield 0.26 g (34%). Anal. calcd. for C<sub>121</sub>H<sub>144</sub>N<sub>6</sub>O<sub>10</sub>: C, 78.88; H, 7.88; N, 4.56, found: C, 78.69; H, 8.01; N, 4.46. UV-vis (DCM): λ<sub>max</sub>, nm (log ε) 263 (4.72), 422 (5.71), 475 (4.60), 506 (4.76), 555 (4.08), 593 (3.75), 651 (3.77). IR (KBr) ν<sub>max</sub>, cm<sup>-1</sup> 3445 (N–H), 2920–2853 (aliphatic-CH), 1770, 1701, 1651, 1597, 1507, 1461, 1358, 1296, 1246, 1165, 1075, 959, 798, 732. <sup>1</sup>H NMR (500 MHz; CDCl<sub>3</sub>; Me<sub>4</sub>Si): δ<sub>H</sub>, ppm -2.79 (2H, s, pyrrole-NH), 0.90–0.88 (15H, m, -CH<sub>3</sub>), 1.50–1.34 (60H, m, -CH<sub>2</sub>-), 1.65–1.61 (6H, m, -CH<sub>2</sub>-), 1.81–1.75 (4H, m, -CH<sub>2</sub>-), 2.04–1.91 (10H, m, -CH<sub>2</sub>-), 3.79–3.75 (2H, m, -N-CH<sub>2</sub>-), 4.25–4.20 (6H, m, -O-CH<sub>2</sub>-), 4.31 (6H, t, -O-CH<sub>2</sub>- and -NH-CH<sub>2</sub>-), 7.03 (1H, t, -CO-NH-), 7.24 (4H, d, Ar-H), 7.26 (2H, s, Ar-H), 8.03 (2H, d, Ar-H), 8.07 (4H, d, Ar-H), 8.08 (2H, d, Ar-H), 8.20 (2H, d, Ar-H), 8.26 (2H, d, Ar-H), 8.32 (4H, d, Ar-H), 8.52 (2H, d, Ar-H), 8.76 (2H, d, Ar-H), 8.86 (6H, s, Ar-H). <sup>13</sup>C NMR (125 MHz; CDCl<sub>3</sub>) δ<sub>C</sub>, ppm 14.0, 14.1, 17.8, 22.6, 22.7, 25.5, 25.7, 26.21, 26.24, 26.8, 28.5, 29.38, 29.47, 29.50, 29.53, 29.67, 29.71, 31.5, 31.9, 33.1, 39.6, 65.8, 68.23, 68.26, 112.7, 118.3, 120.0, 120.3, 121.0, 121.2, 122.2, 122.4, 125.4, 128.4, 128.6, 128.8, 128.9, 130.1, 130.5, 130.8, 131.27, 131.33, 131.5, 131.7, 131.8, 133.9, 134.1, 134.2, 134.6, 134.8, 135.5, 135.6, 145.4, 158.9, 159.0, 163.0, 163.2, 167.6, 168.1. MS (ESI): *m/z* 1865 (calcd. for [M + Na]<sup>+</sup> 1865).

**Synthesis of TPP-C<sub>6</sub>-PIE.** The same procedure as for TPP-C<sub>4</sub>-PIE with **10** (0.5 g, 0.39 mmol), **3** (0.18 g, 0.32 mmol) and imidazole (5 g), to give the title compound as a red solid. Yield 0.27 g (40%). Anal. calcd. for C<sub>123</sub>H<sub>148</sub>N<sub>6</sub>O<sub>10</sub>: C, 78.98; H, 7.98; N, 4.49, found: C, 78.97; H, 8.13; N, 4.56. UV-vis (CH<sub>2</sub>Cl<sub>2</sub>): λ<sub>max</sub>, nm (log ε) 263 (4.79), 422 (5.70), 474 (4.60), 506 (4.76), 555 (4.08), 593 (3.74), 650 (3.75). IR (KBr) ν<sub>max</sub>, cm<sup>-1</sup> 3383–3320 (N–H), 2932–2854 (aliphatic-CH), 1719, 1698, 1650, 1601, 1511, 1470, 1360, 1296, 1250, 1180, 1081, 966, 842, 801, 737. <sup>1</sup>H NMR (500 MHz; CDCl<sub>3</sub>; Me<sub>4</sub>Si): δ<sub>H</sub>, ppm -2.79 (2H, s, pyrrole-NH), 0.90–0.88 (15H, m, -CH<sub>3</sub>), 1.46–1.31 (60H, m, -CH<sub>2</sub>-), 1.69–1.58 (8H, m, -CH<sub>2</sub>-), 1.89–1.77 (10H, m, -CH<sub>2</sub>-), 2.00–1.93 (6H, m, -CH<sub>2</sub>-), 3.66–3.63 (2H, m, -N-CH<sub>2</sub>-), 4.25–4.20 (8H, m, -O-CH<sub>2</sub>- and -NH-CH<sub>2</sub>-), 4.32 (4H, t, -O-CH<sub>2</sub>-), 6.76 (1H, t, -CO-NH-), 7.23 (4H, d, Ar-H), 7.26 (2H, d, Ar-H), 8.00 (2H, d, Ar-H), 8.09–9.05 (6H, m, Ar-H), 8.19 (2H, d, Ar-H), 8.27 (6H, d, Ar-H), 8.48 (2H, d, Ar-H), 8.76 (2H, d, Ar-H), 8.85 (6H, s, Ar-H). MS (ESI): *m/z* 1893 (calcd. for [M + Na]<sup>+</sup> 1893). <sup>13</sup>C NMR (125 MHz; CDCl<sub>3</sub>) δ<sub>C</sub>, ppm 14.0, 14.1, 22.6, 22.7, 25.7, 26.2, 27.00, 27.02, 27.9, 28.5, 29.2, 29.38, 29.49, 29.53, 29.67, 29.72, 31.5, 31.9, 40.3, 40.5, 65.8, 68.28, 68.30, 112.7, 118.2, 120.0, 120.3, 121.5, 121.7, 122.4, 125.3, 125.5, 128.7, 128.8, 129.0, 130.2, 131.0, 131.7, 131.8, 134.1, 134.2, 134.3, 134.7, 135.0, 135.56, 135.61, 145.4, 158.96, 158.98, 163.3, 167.7, 168.2.

**Synthesis of TPP-C<sub>8</sub>-PIE.** The same procedure as for TPP-C<sub>4</sub>-PIE with **11** (1.07 g, 0.79 mmol), **3** (0.55 g, 0.95 mmol) and imidazole (10 g), to give the title compound as a red solid. Yield 0.53 g (38%). Anal. calcd. for C<sub>125</sub>H<sub>152</sub>N<sub>6</sub>O<sub>10</sub>: C, 79.08; H, 8.07; N, 4.43, found: C, 79.04; H, 8.09; N, 4.52. UV-vis (CH<sub>2</sub>Cl<sub>2</sub>): λ<sub>max</sub>, nm (log ε) 263 (4.72), 422 (5.70), 474 (4.59), 506 (4.75), 555 (4.08), 593 (3.75), 650 (3.77). IR (KBr) ν<sub>max</sub>, cm<sup>-1</sup> 3321 (N–H), 2928–2856 (aliphatic-CH), 1701, 1653, 1598, 1505, 1471, 1351, 1290, 1246, 1169, 1078, 965, 799, 738. <sup>1</sup>H NMR (500 MHz; CDCl<sub>3</sub>; Me<sub>4</sub>Si): δ<sub>H</sub>, ppm -2.80 (2H, s, pyrrole-NH), 0.92–0.88 (15H, m, -CH<sub>3</sub>), 1.50–1.31 (66H, m, -CH<sub>2</sub>-), 1.65–1.60 (8H, m, -CH<sub>2</sub>-), 1.82–1.75 (8H, m, -CH<sub>2</sub>-), 2.01–1.94 (6H, m, -CH<sub>2</sub>-), 3.65–3.61 (2H, m, -N-CH<sub>2</sub>-), 4.26–4.17 (8H, m, -O-CH<sub>2</sub>- and -NH-CH<sub>2</sub>-), 4.32 (4H, t, -O-CH<sub>2</sub>-), 6.55 (1H, t, -CO-NH-), 7.24 (4H, d, Ar-H), 7.27 (2H, d, Ar-H), 7.99 (2H, d, Ar-H), 8.07 (4H, d, Ar-H), 8.10 (2H, d, Ar-H), 8.15 (2H, d, Ar-H), 8.23 (4H, d, Ar-H), 8.27 (2H, d, Ar-H), 8.46 (2H, d, Ar-H), 8.76 (2H, d, Ar-H), 8.87–8.85 (6H, m, Ar-H). <sup>13</sup>C NMR (125 MHz; CDCl<sub>3</sub>) δ<sub>C</sub>, ppm 14.0, 14.1, 22.6, 22.7, 25.7, 26.2, 26.4, 26.5, 27.8, 28.5, 29.39, 29.45, 29.49, 29.50, 29.54, 29.68, 29.72, 31.5, 31.9, 40.0, 40.1, 65.8, 68.26, 68.28, 112.7, 118.3, 120.0, 120.3, 121.4, 121.5, 122.4, 125.4, 128.6, 129.0, 130.2, 130.9, 131.7, 131.8, 134.08, 134.14, 134.23, 134.7, 134.9, 135.5, 135.6, 145.4, 158.93, 158.95, 163.3, 167.7, 168.2. MS (ESI): *m/z* 1921 (calcd. for [M + Na]<sup>+</sup> 1921).

**Synthesis of TPP-C<sub>10</sub>-PIE.** The same procedure as for TPP-C<sub>4</sub>-PIE with **12** (0.57 g, 0.41 mmol), **3** (0.29 g, 0.49 mmol) and imidazole (5 g), to give the title

compound as a red solid. Yield 0.26 g (34%). Anal. calcd. for C<sub>127</sub>H<sub>156</sub>N<sub>6</sub>O<sub>10</sub>: C, 79.17; H, 8.16; N, 4.36, Found: C, 79.07; H, 8.11; N, 4.41. UV-vis (CH<sub>2</sub>Cl<sub>2</sub>): λ<sub>max</sub>, nm (log ε) 263 (4.73), 422 (5.70), 473 (4.58), 505 (4.75), 556 (4.08), 593 (3.74), 651 (3.77). IR (KBr) ν<sub>max</sub>, cm<sup>-1</sup> 3426 (N–H), 2922–2852 (aliphatic-CH), 1697, 1650, 1607, 1511, 1469, 1385, 1296, 1248, 1171, 1081, 1026, 798. <sup>1</sup>H NMR (500 MHz; CDCl<sub>3</sub>; Me<sub>4</sub>Si): δ<sub>H</sub>, ppm -2.84 (2H, s, pyrrole-NH), 0.92–0.88 (15H, m, -CH<sub>3</sub>), 1.47–1.31 (70H, m, -CH<sub>2</sub>-), 1.66–1.62 (8H, m, -CH<sub>2</sub>-), 1.82–1.76 (8H, m, -CH<sub>2</sub>-), 2.00–1.93 (6H, m, -CH<sub>2</sub>-), 3.66–3.62 (2H, m, -N-CH<sub>2</sub>-), 4.17 (2H, t, -NH-CH<sub>2</sub>-), 4.26–4.22 (6H, m, -O-CH<sub>2</sub>-), 4.32 (4H, t, -O-CH<sub>2</sub>-), 6.53 (1H, t, -CO-NH-), 7.28–7.25 (6H, m, Ar-H), 8.02–8.00 (2H, m, Ar-H), 8.09–8.07 (6H, m, Ar-H), 8.15 (2H, d, Ar-H), 8.25–8.19 (4H, m, Ar-H), 8.26 (2H, d, Ar-H), 8.44–8.41 (2H, m, Ar-H), 8.75 (2H, d, Ar-H), 8.87 (6H, s, Ar-H). <sup>13</sup>C NMR (125 MHz; CDCl<sub>3</sub>) δ<sub>C</sub>, ppm 14.0, 14.1, 22.6, 22.7, 25.7, 26.2, 27.0, 27.1, 28.0, 28.5, 29.2, 29.3, 29.4, 29.5, 29.7, 31.5, 31.9, 40.4, 40.5, 65.8, 68.3, 112.7, 118.2, 120.0, 120.3, 121.5, 121.8, 122.4, 125.2, 125.5, 128.7, 128.8, 129.1, 130.2, 131.0, 131.7, 131.8, 134.2, 134.3, 134.7, 135.0, 135.59, 135.61, 145.5, 159.0, 163.4, 167.7, 168.2. MS (ESI): *m/z* 1949 (calcd. for [M + Na]<sup>+</sup> 1949).

**Synthesis of TPP-C<sub>12</sub>-PIE.** The same procedure as for TPP-C<sub>4</sub>-PIE with **13** (0.47 g, 0.34 mmol), **3** (0.16 g, 0.28 mmol) and imidazole (5 g), to give the title compound as a red solid. Yield 0.25 g (40%). Anal. calcd. for C<sub>129</sub>H<sub>160</sub>N<sub>6</sub>O<sub>10</sub>: C, 79.26; H, 8.25; N, 4.30, found: C, 79.08, H, 8.26, N, 4.34. UV-vis (CH<sub>2</sub>Cl<sub>2</sub>): λ<sub>max</sub>, nm (log ε) 263 (4.72), 422 (5.69), 474 (4.57), 506 (4.73), 556 (4.08), 594 (3.74), 651 (3.76). IR (KBr) ν<sub>max</sub>, cm<sup>-1</sup> 3445 (N–H), 2926–2850 (aliphatic-CH), 1699, 1655, 1605, 1505, 1462, 1351, 1294, 1246, 1171, 1076, 966, 800, 729. <sup>1</sup>H NMR (500 MHz; CDCl<sub>3</sub>; Me<sub>4</sub>Si): δ<sub>H</sub>, ppm -2.90 (2H, s, pyrrole-NH), 0.92–0.88 (15H, m, -CH<sub>3</sub>), 1.46–1.31 (74H, m, -CH<sub>2</sub>-), 1.65–1.60 (8H, m, -CH<sub>2</sub>-), 1.83–1.72 (8H, m, -CH<sub>2</sub>-), 2.00–1.95 (6H, m, -CH<sub>2</sub>-), 3.65–3.61 (2H, m, -N-CH<sub>2</sub>-), 4.12 (2H, t, -NH-CH<sub>2</sub>-), 4.25–4.22 (6H, m, -O-CH<sub>2</sub>-), 4.33 (4H, t, -O-CH<sub>2</sub>-), 6.49 (1H, t, -CO-NH-), 7.27 (6H, d, Ar-H), 8.04–8.00 (4H, m, Ar-H), 8.12–8.07 (6H, m, Ar-H), 8.14 (2H, d, Ar-H), 8.21–8.18 (2H, m, Ar-H), 8.32–8.27 (4H, m, Ar-H), 8.75 (2H, d, Ar-H), 8.83 (4H, s, Ar-H), 8.86 (2H, d, Ar-H). <sup>13</sup>C NMR (125 MHz; CDCl<sub>3</sub>) δ<sub>C</sub>, ppm 14.0, 14.1, 22.6, 22.7, 25.7, 26.2, 27.1, 27.2, 28.0, 28.5, 29.28, 29.33, 29.38, 29.47, 29.50, 29.54, 29.57, 29.68, 29.72, 31.5, 31.9, 40.4, 40.5, 65.8, 68.3, 112.69, 112.71, 118.2, 120.0, 120.3, 121.3, 121.6, 122.3, 125.2, 125.3, 128.5, 128.7, 129.0, 130.2, 130.8, 131.7, 131.8, 134.13, 134.18, 134.21, 134.7, 134.8, 135.60, 135.63, 145.5, 159.0, 163.2, 167.7, 168.2. MS (ESI): *m/z* 1977 (calcd. for [M + Na]<sup>+</sup> 1977).

## CONCLUSION

Novel dyads TPP-C<sub>*n*</sub>-PIE (*n* = 4, 6, 8, 10 and 12) were synthesized and fully characterized. The UV-vis spectra

revealed these dyads have broad optical absorption from the ultraviolet region to the visible region, due to the complementary absorption of porphyrin and perylene units. DSC traces and POM textures showed all these dyads have mesogenic properties, and they formed face-on alignment on the slide when cooled. When excited at 423 or 473 nm, the photoluminescent emission showed a Förster and Dexter type energy transfer from the perylene unit to the porphyrin unit. At the same time, the fluorescence quenching degree of porphyrin units increased as the spacers got shorter. This quenching was ascribed to intramolecular photoinduced electron transfer processes. In these processes, the charge-separated states of molecules,  $\text{TPP}^{\bullet+}\text{-C}_n\text{-PIE}^{\bullet-}$ , were formed, which were further confirmed by the photocurrent generation. These behaviors made the dyads candidates for single-component photovoltaic active materials.

### Supplementary information

The DSC curves,  $^1\text{H}$ - and  $^{13}\text{C}$ -NMR, IR and MS spectra of the dyads are supplied as supplementary information.

### Acknowledgments

We gratefully acknowledge financial support from the Natural Science Foundation of China (No. 11364013), Opening Fund of Guangxi Key Laboratory of Electrochemical and Magnetochemical Functional Materials (EMFM20181101), and the Special Funding for Distinguished Expert from Guangxi Zhuang Autonomous Region. We thank Guangxi Key Laboratory of Hidden Metallic Ore Deposits Exploration for providing support to the POM measurements.

### REFERENCES

- Cheng P and Zhan X. *Chem. Soc. Rev.* 2016; **45**: 2544–2582.
- Heeger AJ. *Adv. Mater.* 2014; **26**: 10–28.
- Kim JY, Lee K, Coates NE, Moses D, Nguyen TQ, Dante M and Heeger AJ. *Science* 2007; **317**: 222–225.
- Tang CW. *Appl. Phys. Lett.* 1986; **48**: 183–185.
- Zhao J, Li Y, Yang G, Jiang K, Lin H, Ade H, Ma W and Yan H. *Nat. Energy* 2016; **1**: 15027.
- Deng D, Zhang Y, Zhang J, Wang Z, Zhu L, Fang J, Xia B, Wang Z, Lu K, Ma W and Wei Z. *Nat. Commun.* 2016; **7**: 13740.
- Vohral V, Kawashima K, Kakara T, Koganezawa T, Osaka I, Takimiya K and Murata H. *Nat. Photonics* 2015; **9**: 403–408.
- Zhao W, Qian D, Zhang S, Li, Inganas O, Gao F and Hou J. *Adv. Mater.* 2016; **28**: 4734–4739.
- Yang Y, Zhang ZG, Bin H, Chen S, Gao L, Xue L, Yang C and Li Y. *J. Am. Chem. Soc.* 2016; **138**: 15011–15018.
- Zhao W, Li S, Yao H, Zhang S, Zhang Y, Yang B and Hou J. *J. Am. Chem. Soc.* 2017; **139**: 7148–7151.
- Roncali J. *Adv. Energy Mater.* 2011; **1**: 147–160.
- Nguyen TL, Lee TH, Gautam B, Park SY, Gundogdu K, Kim JY and Woo HY. *Adv. Funct. Mater.* 2017; 1702474.
- Bullock JE, Carmieli R, Mickley SM, Vura-Weis J and Wasielewski MR. *J. Am. Chem. Soc.* 2009; **131**: 11919–11929.
- Lai W, Li C, Zhang J, Yang F, Colberts FJM, Guo B, Wang QM, Li M, Zhang A, Janssen RA, Zhang M and Li W. *Chem. Mater.* 2017; **29**: 7073–7077.
- Narayananaswamy K, Venkateswararao A, Nagarjuna P, Bishnoi S, Gupta V, Chand S and Singh SP. *Angew. Chem. Int. Ed.* 2016; **55**: 12334–12337.
- Koyuncu S, Wang HW, Liu F, Toga KB, Gu W and Russell TP. *J. Mater. Chem. A.* 2014; **2**: 2993–2998.
- Guo C, Lin YH, Witman MD, Smith KA, Wang C, Hexemer A, Strzalka J, Gomez ED and Verduzco R. *Nano Lett.*, 2013; **13**: 2957–2963.
- Izawa S, Hashimoto K and Tajima K. *Phys. Chem. Chem. Phys.* 2012; **14**: 16138–16142.
- Nierengarten JF, Eckert JF, Nicoud JF, Ouali L, Krasnikov V and Hadziioannou G. *Chem. Commun.* 1999; 617–618.
- Hartnett PE, Dyar SM, Margulies EA, Shoer LE, Cook AW, Eaton SW, Marks TJ and Wasielewski MR. *Chem. Sci.* 2015; **6**: 402–411.
- Dossel LF, Kamm V, Howard IA, Laquai F, Pisula W, Feng X, Li C, Takase M, Kudernac T, Feyter SD and Mullen K. *J. Am. Chem. Soc.* 2012; **134**: 5876–5886.
- Kumar M and Kumar S. *Polym. J.* 2016; **49**: 85–111.
- Wohrle T, Wurzbach I, Kirres J, Kostidou A, Kapernaum N, Litterscheidt J, Haenle JC, Staffeld P, Baro A, Giesselmann F and Laschat S. *Chem. Rev.* 2016; **116**: 1139–1241.
- Pal SK, Setia S, Avinash BS and Kumar S. *Liq. Cryst.* 2013; **40**: 1769–1816.
- Kumar S. *Liq. Cryst.* 2004; **31**: 1037–1059.
- Sergeyev S, Pisula W and Geerts YH. *Chem. Soc. Rev.* 2007; **36**: 1902–1929.
- Laschat S, Baro A, Steinke N, Giesselmann F, Hagele C, Scalia G, Judele R, Kapatsina E, Sauer S, Schreivogel A and Tosoni M. *Angew. Chem. Int. Ed.* 2007; **46**: 4832–4887.
- Boden N, Bushby RJ and Clements F. *J. Chem. Phys.* 1993; **98**: 5920–5931.
- Lee KJ, Woo JH, Xiao Y, Kim E, Mazur LM, Kreher D, Attias AJ, Matczyszyn K, Samoc M, Heinrich B, Mery S, Fages F, Mager L, Daleo A, Wu JW, Mathivet F, Andre P and Ribierre JC. *RSC Adv.* 2016; **6**: 57811–57819.
- Kong X, Xia L, Zhang H, Dai S, Yu C, Liu Z, Mu L, Wang G and He Z. *RSC Adv.* 2017; **7**: 17030–17037.

31. Lee KJ, Woo JH, Kim E, Xiao Y, Su X, Mazur LM, Attias AJ, Fages F, Cregut O, Barsella A, Mathevet F, Mager L, Wu JW, Daleo A and Ribierre JC. *Phys. Chem. Chem. Phys.* 2016; **18**: 7875–7887.
33. Kong X, Liu P, Wang G, Xia L, Dai S, Su J, Liao P, Liu Z and Mu L. *Chin. J. Org. Chem.* 2016; **36**: 1325–1334.
34. Zhao KQ, An LL, Zhang XB, Yu WH, Hu P, Wang BQ, Xu J, Zeng QD, Monobe H, Shimizu Y, Heinrich B and Donnio B. *Chem. Eur. J.* 2015; **12**: 10379–10390.
35. Xiao Y, Su X, Sosa-Vargas L, Lacaze E, Heinrich B, Donnio B, Kreher D, Mathevet F and Attias AJ. *CrystEngComm.* 2016; **18**: 4787–4798.
36. Kumar S, Naidu J and Varshney SK. *Mol. Cryst. Liq. Cryst.* 2004; **411**: 355–362.
37. Varshney SK, Nagayama H, Prasad V, and Takezoe H. *Mol. Cryst. Liq. Cryst.* 2010; **517**: 97–112.
38. Kong X, He Z, Zhang Y, Mu L, Liang C, Chen B, Jing X and Cammidge AN. *Org. Lett.* 2011; **13**: 764–767.
39. Guo H, Zhu M, Wang Z and Yang F. *Tetrahedron Lett.* 2016; **57**: 4191–4195.
40. Fang X, Guo H, Lin J and Yang F. *Tetrahedron Lett.* 2016; **57**: 4939–4943.
41. Gupta SK, Setia S, Sidiq S, Gupta M, Kumar S and Pal SK, *RSC Adv.* 2013; **3**: 12060–12065.
42. Kong X, Dai S, Wang G, Zhang Z, Zhang L, Liao P and Liu W, *Mol. Cryst. Liq. Cryst.* 2017; **650**: 56–64.
43. Kadish KM, Smith KM and Guillard R. *The Porphyrin Handbook: Applications: Past, Present, and Future*, Vol. 6. Academic Press: San Diego, CA, 1999; 62–72.
44. Miloslav M, Jiri D, Pavel C, Magda V, Lenka H, Adela J, Pavel K, Tomas S, Veronika N and Petr Z. *J. Med. Chem.* 2016; **59**: 9443–9456.
45. Lovell JF, Chan MW, Qi Q, Chen J and Zheng G. *J. Am. Chem. Soc.* 2011; **133**: 18580–18582.
46. Yella A, Lee HW, Tsao HN, Yi C, Chandiran AK, Nazeeruddin MK, Diau EWG, Yeh CY, Zakeeruddin SM and Gratzel M. *Science* 2011; **334**: 629–634.
47. Wang CL, Hu JY, Wu CH, Kuo HH, Chang YC, Lan ZJ, Wu HP, Diau EWG and Lin CY. *Energy Environ. Sci.* 2014; **7**: 1392–1396.
48. Qin H, Li L, Guo F, Su S, Peng J, Cao Y and Peng X. *Energy Environ. Sci.* 2014; **7**: 1397–1401.
49. Walter MG, Rudine AB and Wamser CC. *J. Porphyrins Phthalocyanines* 2010; **14**: 759–792.
50. Di D, Yang L, Richter JM, Meraldi L, Altamimi RM, Alyamani AY, Credgington D, Musselman KP, MacManus-Driscoll JL and Friend RH. *Adv. Mater.* 2017; **29**: 1605987.
51. Gupta RK, Das D, Gupta M, Pal SK, Iyer PK and Achalkumar AS. *J. Mater. Chem. C* 2017; **5**: 1767–1781.
52. Xiong Y, Wu B, Zheng X, Zhao Z, Deng P, Lin M, Tang B and Ong BS. *Adv. Sci.* 2017; **4**: 1700110.
53. Wang Z, Zheng N, Zhang W, Yan H, Xie Z, Ma Y, Huang F and Cao Y. *Adv. Energy Mater.* 2017; **7**: 1700232.
54. Bin H, Yang Y, Zhang ZG, Ye L, Ghasemi M, Chen S, Zhang Y, Zhang C, Sun C, Xue L, Yang C, Ade H and Li Y. *J. Am. Chem. Soc.* 2017; **139**: 5085–5094.
55. Mo X, Shi MM, Huang JC, Wang M and Chen HZ. *Dyes Pigm.* 2008; **76**: 236–242.
56. Ernst F, Heek T, Setaro A, Haag R and Reich S. *J. Phys. Chem. C* 2013; **117**: 1157–1162.
57. Brun A and Etemad-Moghadam G. *Synthesis*, 2002, 1385–1390.
58. Charisiadis A, Nikolaou V, Karikis K, Giatagana C, Chalepli K, Ladomenou K, Biswas S, Sharma GD and Coutsolelos AG. *New J. Chem.* 2016; **40**: 5930–5941.
59. Adler AD. *J. Org. Chem.* 1967; **32**: 476.
60. Chou WC, Tan CW, Chen SF and Ku H. *J. Org. Chem.* 1998; **63**: 10015–10017.
61. Thelakkat M and Schmidt H. *Adv. Mater.* 1998; **10**: 219–223.
62. Zhang Y, Hanifi DA, Fernandez-Liencrez MP, Klivansky LM, Ma B, Navarro A and Liu Y. *ACS Appl. Mater. Inter.* 2017; **9**: 20010–20019.
63. Wasbotten IH, Conradie J and Ghosh A. *J. Phys. Chem. B* 2003; **107**: 3613–3623.
64. Lakowicz JR. *Principles of Fluorescence Spectroscopy* (3rd edn), Springer Science+Business Media, LLC: New York, 2006; 332–336.